

¹H NMR Relaxometry Study of a Rod-Like Chiral Liquid Crystal in Its Isotropic, Cholesteric, TGBA*, and TGBC* Phases

Tomaž Apih,[†] Valentina Domenici,^{*,‡} Anton Gradišek,[†] Vera Hamplová,[§] Miroslaw Kaspar,[§] Pedro J. Sebastião,^{||} and Marija Vilfan^{†,⊥}

Department of Solid State Physics, Jožef Stefan Institute, Jamova 39, 1000 Ljubljana, Slovenia, Dipartimento di Chimica e Chimica Industriale, Università degli studi di Pisa, via Risorgimento 35, 56126 Pisa, Italy, Institute of Physics, Academy of Sciences of the Czech Republic, Na Slovance 2, 182 21 Prague, Czech Republic, Departamento de Física, TU Lisbon, Av. Rovisco Pais 1, 1049-001 Lisboa, Portugal, and Centro de Física da Matéria Condensada, Complexo Interdisciplinar da Universidade de Lisboa, Av. Prof. Gama Pinto, 2-P-1649-003 Lisboa, Portugal

Received: June 7, 2010; Revised Manuscript Received: August 13, 2010

The molecular dynamics of a chiral liquid crystal showing a rich variety of frustrated mesophases has been investigated by means of ¹H NMR relaxometry. The interest in this lactate derivative, HZL 7/*, is related to a large range of thermal stabilities of the twist grain boundary (TGB) phases. Dispersions of the ¹H spin-lattice relaxation times, T_1 , in the frequency range from 300 MHz to 5 kHz were measured and consistently analyzed in the isotropic, chiral nematic, TGBA*, and two TGBC* phases. In the isotropic and N* phases, a three-exponential magnetization decay was observed and assigned to three specific molecular groups of the HZL 7/* (molecular core, methyl, and methylene groups). In the TGB phases, all T_1 components merge into a single one. The analysis of the T_1 dispersion in the TGBA* phase shows that the translational self-diffusion relaxation mechanism dominates over a broad frequency range and that layer undulations are less relevant than the relaxation contribution associated with the diffusion process across the TGB structure. In the TGBC₁* phase, the T_1 dispersion presents a strong contribution of in-layer tilt direction fluctuations ($T_1^{-1} \propto \nu^{-1/2}$), while, in the TGBC₂* phase, the linear frequency dependence of T_1 could be associated with a much stronger contribution of layer undulations than for the other TGB phases. This is at present the first molecular dynamics investigation on several TGB phases by means of ¹H NMR relaxometry.

1. Introduction

Liquid crystalline phases defined as “frustrated” ones¹ attracted the interest of the scientific community in view of the many possible applications deriving from the manipulation of their structures by application of external fields. Among these, the blue phases² are characterized by an isotropic structure,³ while the so-called twist grain boundary (TGB) phases,² predicted theoretically by Renn and Lubensky⁴ and observed experimentally for the first time by Goodby et al.,⁵ have an anisotropic structure. Different materials have been synthesized showing several kinds of TGB phases, with tilted⁶ (TGBC*) and untilted (TGBA*) molecules in the smectic layer blocks. Experimental studies have been performed in order to characterize the structure, molecular order, and dynamics of both TGBA* and TGBC* phases by means of calorimetry,⁷ dielectric spectroscopy,⁸ X-ray measurements,⁹ and NMR spectroscopy.^{10–13}

The basic features of the supramolecular structure of the TGBA* are well-known. They are illustrated in Scheme 1: the molecules (colored rods) are locally packed in SmA-like blocks which are arranged in a helical way along an axis perpendicular to the local phase director, \vec{n} . Two adjacent blocks are rotated by an angle ϕ and separated by a “grain boundary”, containing

equidistant dislocation or disclination lines (see the gray lines in Scheme 1). The TGB block length is l_b . Another feature of the TGBA* phase is the helical pitch, $P = (2\pi/\phi)l_b$, in which the ratio $2\pi/\phi$ indicates the TGBA* periodicity (and the number of blocks for each helical slab).⁶ This structure is very sensitive to the unwinding or strong distortions by external electric¹⁴ or magnetic fields.^{13,15} Different from the TGBA* phase, TGBC* of different kinds are known to exhibit various supramolecular structures. All of them, however, have in common the presence of a molecular tilt with respect to the local nematic director, \vec{n} , commonly referred as the θ angle. In Scheme 1, one of the proposed TGBC* phase structures, where the characteristic TGBC* blocks have the same structure as the ferroelectric SmC* phase,⁶ is represented. This TGBC* structure is most probably the one exhibited by the sample under investigation in this work.

Few studies exist about the dynamic properties of the TGB phases. Most of them are based on dielectric spectroscopy⁸ and indicate some general features about the collective motions. In particular, the “soft mode” observed in the TGBA* phase is always weaker than that in the SmA phase, and the “Goldstone mode”, which affects the TGBC* phase, is strongly reduced with respect to the SmC* phase.^{8,16} Moreover, in the range of frequencies where the dielectric relaxation is dominated by the collective motional contributions (<100 kHz), discontinuities have been observed at the transitions between the TGB phases in the N*-TGB-SmC* phase sequence. Similar conclusions could be drawn on the basis of dynamic light scattering studies.¹⁷ Information about the local molecular motions, such as the overall reorientational molecular motions (spinning and tum-

* Corresponding author. Phone: 0039 050 2219 215. Fax: 0039 050 2219 260. E-mail: valentin@deci.unipi.it.

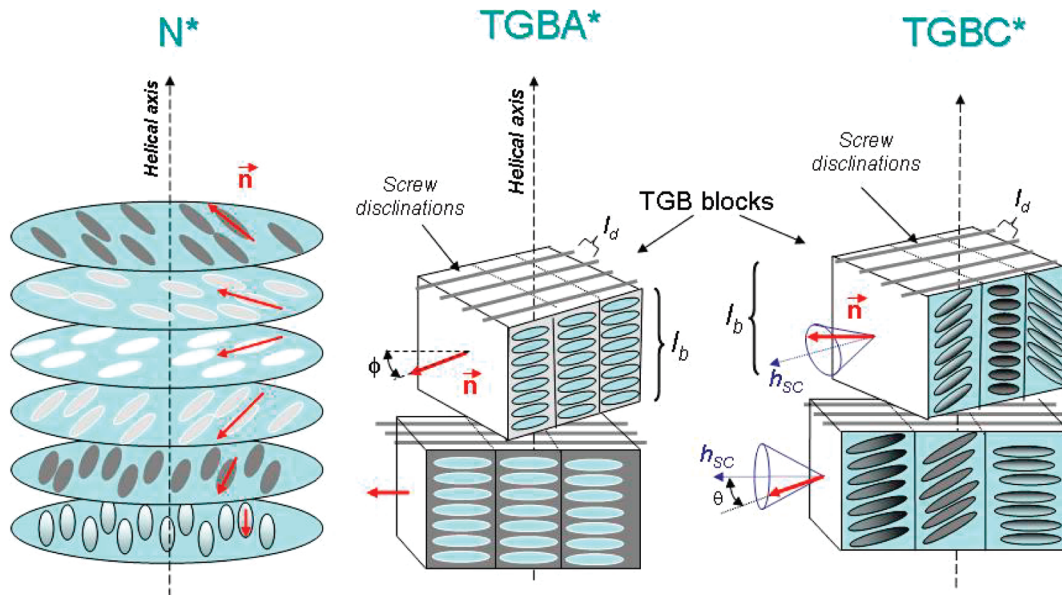
[†] Jožef Stefan Institute.

[‡] Università degli studi di Pisa.

[§] Academy of Sciences of the Czech Republic.

^{||} TU Lisbon and Complexo Interdisciplinar da Universidade de Lisboa.

[⊥] Deceased.

SCHEME 1: Basic Schematic Representation of the N*, TGBA*, and TGBC* Phases^a

^a Red arrows indicate the local mesophase director, \vec{n} . The helical axis of the phases is also displayed. The dimensions of the TGB blocks (l_b), the distance (l_d) between consecutive screw disclinations (gray lines), and the twist angle between two consecutive blocks in the TGB phases (ϕ) are indicated. The tilt angle (θ) and the helical axis (h_{SC}) of the SmC* structure within the TGBC* phase are displayed.

bling) and molecular translational self-diffusion, can be obtained by means of NMR spectroscopy.^{18,19} For instance, the line-shape analysis of ²H NMR spectra recorded by means of a 2D exchange NMR sequence²⁰ in the TGBA* phase of a chiral compound allowed Zhang et al.¹¹ to estimate the self-diffusion constant $D_{||}$ along the helical pitch to be about $10^{-12} \text{ m}^2/\text{s}$.²¹ Fast field cycling NMR relaxometry^{22,23} has also been used to investigate another LC compound that presents a stable TGBA* phase in a very small temperature range.²⁴ It was reported that the observed behavior of ¹H spin-lattice relaxation time in the low frequency regime was due to molecular dynamics specific for this mesophase. However, it is not possible to generalize these results in view of the narrow temperature stability range of the TGBA* phase observed in both cases.^{11,24} To our knowledge, the present work is the first molecular dynamics investigation by means of ¹H NMR relaxometry of different TGB phases, stable in a wide temperature range.

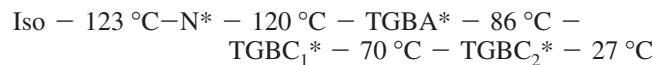
The recent advances in NMR relaxometry techniques^{25,26} have made it possible to measure the proton spin-lattice relaxation time T_1 over a wide range of Larmor frequencies, typically from a few kHz to hundreds of MHz, enabling one to probe various molecular motions. The region of narrowing regime of motions is usually dominated by single molecular motions, overall and internal ones, and it corresponds to frequencies higher than tens of MHz. In this frequency region, translational self-diffusion can also be an effective relaxation mechanism.²⁴ However, NMR relaxometry is quite a unique technique for the detection of slow motions, such as collective motions, that contribute to the relaxation in the kilohertz region. Among those, order director fluctuations (ODF), in nematic phases, and layer undulations (LU), in SmA phases (see Scheme 2), have been widely explored by these techniques in several liquid crystalline systems.^{23,26} Rotations mediated by translational displacements (RMTD) have also been studied by NMR relaxometry.^{23,26}

In this paper, we report a comprehensive proton NMR relaxation study on the chiral rod-like mesogen containing the (S)-2-methylbutyl-(S)-lactate unit in the chiral chain, named HZL 7/*, presented in Scheme 3.¹² This sample presents an interesting phase sequence—isotropic (I), chiral nematic (N*), TGBA*, and

two TGBC* phases. Different from most of the cases reported in the literature so far, the TGB mesophases shown by the HZL 7/* sample are stable over a wide range of temperatures, making the molecular dynamics investigation possible not only at the phase transitions but also within the temperature domain of each phase.

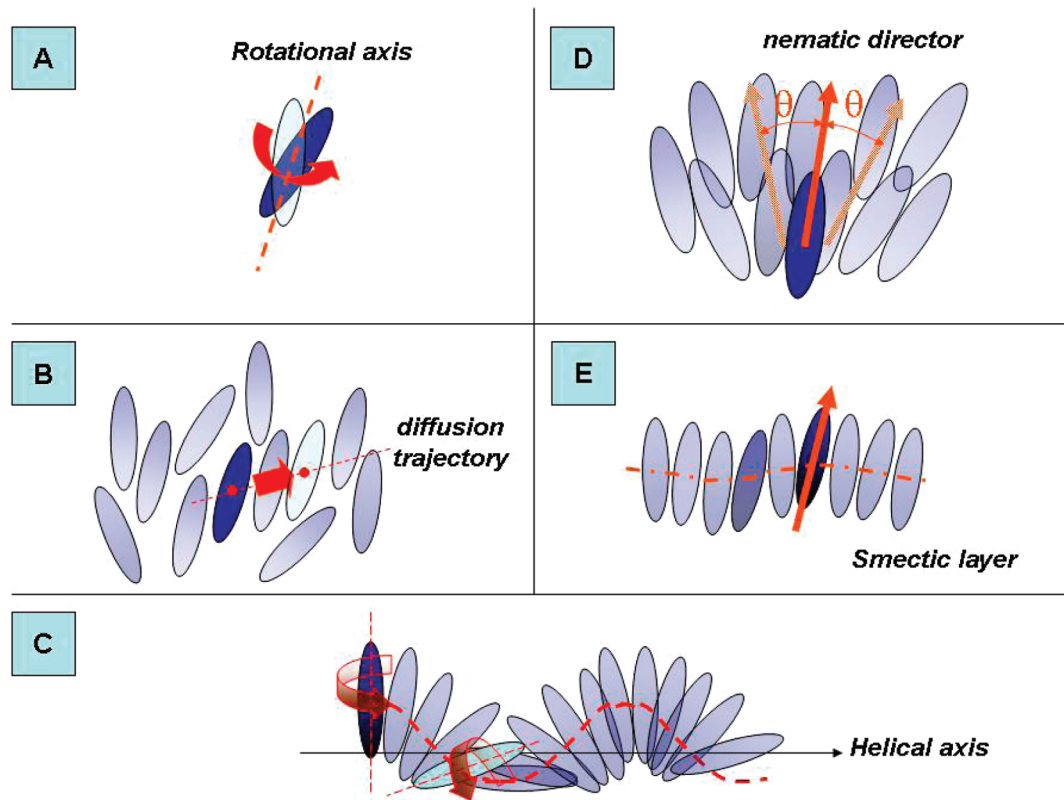
2. Experimental Section

2.1. Materials. The molecular structure of HZL 7/* is reported in Scheme 3. This chiral compound was synthesized according to the procedure reported in ref 12. The level of purity of the sample is $\sim 100\%$ (determined by HPLC chromatography and NMR). Basic chemical and physical characterization of this sample, and of the isotopomer selectively deuterium-labeled on the phenyl ring, namely, HZL 7/*-D₂, has been previously performed by means of polarizing microscopy and X-ray and dielectric spectroscopy.¹² Moreover, the orientational and structural properties of the frustrated mesophases of HZL 7/* were investigated by means of ²H and ¹³C NMR spectroscopy.^{13,15} These studies allowed us to obtain the local orientational order parameters in the mesophases and to study the effect of high magnetic fields on the supramolecular structure of the TGB phases. The temperature transitions have been determined by DSC and polarizing microscopy on cooling the non-labeled sample from the isotropic phase to the crystalline phase as follows:¹²

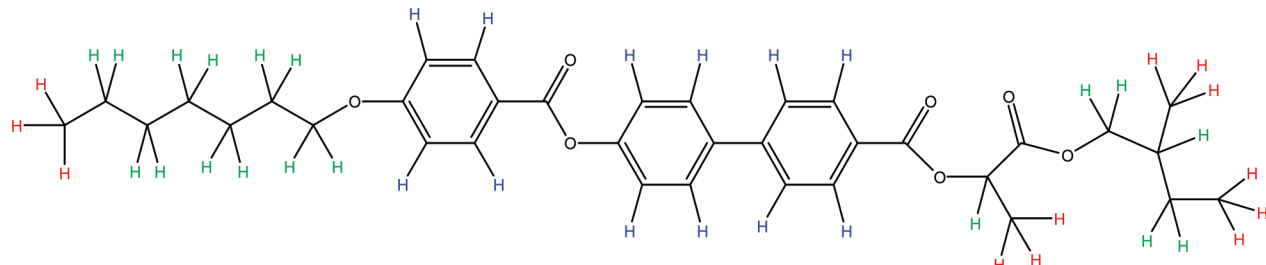


As reported in a previous work,¹³ the HZL 7/* sample is very sensitive to the cooling/heating rates that affect the observed temperature transitions and determine the occurrence of the biphasic regions. Moreover, the presence of the magnetic field may also influence the mesophase behavior,¹⁵ which, in the present study, was determined by measuring the proton NMR relaxation times under different heating/cooling processes:

SCHEME 2: Main Molecular Motions, Detectable by Means of ^1H NMR Relaxometry: (A) Rotations/Reorientations (R); (B) Translational Self-Diffusion (SD); (C) Rotations Mediated by Translational Displacements along the Helical Axis (RMTD); (D) Order Director Fluctuations (ODF); (E) Layer Undulations (LU)



SCHEME 3: Molecular Structure of the Chiral Liquid Crystal HZL 7^a



^a All protons present in the molecule are indicated with different colors: CH₃ (12 protons) are in red, aromatic CH (12 protons) are in blue, and aliphatic CH₂ and CH (18 protons) are in green.

Iso – 120 °C – biphasic – 118 °C – N* – 115 °C –
biphasic – 112 °C – TGBA* – 83 °C ± 2 °C –
TGBC₁* – 60 °C ~ TGBC₂* ~ 40 °C

2.2. ^1H NMR Relaxation Measurements. The relaxation dispersion data were acquired in the Fast Field Cycling NMR relaxometer SPINMASTER FFC-2000 (Stelar s.l.r.). The longitudinal spin-lattice relaxation time T_1 was measured in the frequency range from 16 MHz to 5 kHz in the temperature range from 150 to 40 °C, in several cooling runs. Temperature was controlled with a standard gas flow system with a precision of 0.1 °C. About 600 mg of sample HZL 7^{*} was inserted in a standard 10 mm NMR tube. For frequencies higher than 8 MHz, a non-prepolarized pulse sequence (NPS) was used, while below that frequency relaxation times were obtained using a prepolarized pulse sequence (PPS). The prepolarization and acquisition frequencies were 16.00 and 9.25 MHz, respectively. A 6.5 μs proton 90 ° pulse and a maximum value of the recycle delay of 1.3 s were used. All other parameters were optimized

according to each experiment. Additionally, the proton T_1 values were measured by the inversion recovery pulse sequence in the same temperature range at 100 MHz, using a homemade NMR spectrometer equipped with an Oxford magnet (4.5 μs 90° pulse), and at 300 MHz, using a Bruker NMR Advance II spectrometer (5.2 μs 90° pulse). All relaxation rates were determined by fitting the magnetization decays as a function of variable delay, τ . The fitting procedure is discussed in section 4.

2.3. Data Analysis. ^1H NMR relaxation times T_1 were obtained by analyzing the recorded magnetization decay data with home-written packages working with the software MATLAB version 6.5. The analysis of the relaxation dispersion curves was performed by a global minimum least-squares target fitting procedure using a home-written nonlinear fitting routine.²⁷

3. Theoretical Background

In this section, we present the models used for the analysis of the ^1H NMR dispersion curves obtained in the different

mesophases. A complete treatment of molecular dynamics in liquid crystals can be found in the literature.^{23,28–31}

The total spin-lattice relaxation rate of the investigated system is defined as a sum of the contributions corresponding to the different relaxation mechanisms:

$$T_1^{-1}(\omega) = \sum_i \left(\frac{1}{T_{1i}} \right), \quad i = R, SD, ODF, LU, RMTD \quad (1)$$

where R stands for local molecular rotations/reorientations, SD stands for translational self-diffusion, ODF stands for order director fluctuations, LU stands for layer undulations, and RMTD stands for rotations mediated by translational displacements.

In the case of complex anisotropic molecules, local molecular reorientations can be described, as a first approximation, by a sum of Bloembergen, Purcell, and Pound (BPP) relaxation equations, each one dependent on a correlation time and a prefactor.³² The translational self-diffusion can be analytically modeled in the isotropic phase,³³ while it has to be calculated numerically³⁴ for the liquid crystalline phases. This contribution depends mainly on the correlation time for the translational displacements and on the distance of closest approach between molecules. The correlation times for the rotations/reorientations and translational self-diffusion are thermal activation mechanisms that depend on activation energies.

The collective motions often observed in liquid crystals are order director fluctuations and layer undulations. The former are typically observed in nematic phases and are characterized by a spin-lattice relaxation that depends on frequency as $T_1^{-1} \sim \omega^{-1/2}$.^{35,36} The latter is a type of collective motions usually observed in smectic A phases, and the relaxation rate presents a linear frequency dependence, $T_1^{-1} \sim \omega^{-1}$.³⁶ For both models, their characteristic frequency dependencies are modified in the limit cases of frequencies above or below given high or low cutoff frequency values, respectively. In the low frequency limit, the relaxation rates become frequency independent. In the high frequency limit, both relaxation rates present the same frequency dependence, $T_1^{-1} \sim \omega^{-2}$. The prefactors of both models and the cutoff frequencies depend on the temperature, nematic order parameter, viscoelastic-properties, coherence lengths, and/or molecular dimensions.

In the SmC phases, in addition to LUs, it is possible to observe in-layer order collective fluctuations of the molecular tilting direction (*c*-director fluctuations).³⁵

In chiral systems, molecular translational displacements and molecular rotational motions can be mutually affected by the local structure.^{24,30,36,37} In the case of chiral nematic phases, a model has been proposed to take into account the effect of the rotations mediated by the translational displacements (RMTD) along the helical axis of the chiral system (see Scheme 2):

$$(T_1^{-1})_{\text{RMTD}} = A_{\text{RMTD}} \frac{2\tau_{\text{RMTD}}}{1 + 4\omega^2\tau_{\text{RMTD}}^2} \quad (2)$$

where A_{RMTD} depends on the interproton distance and τ_{RMTD} is the correlation time for this relaxation mechanism. In the case of TGBA phases, the RMTD process across the grain boundaries between the SmA blocks might be described by the same model or by a more detailed and specific model for this type of phases.²⁴

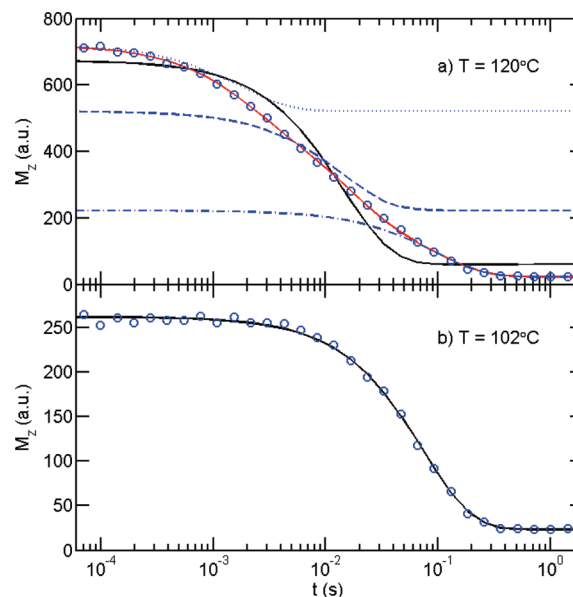


Figure 1. Magnetization decay (empty blue circles) at (a) $T = 120$ °C (isotropic phase) and (b) $T = 102$ °C (TGBA* phase), recorded at $v_L = 25$ kHz. The monoexponential fits (solid black lines) properly describe the magnetization decay only in the TGBA* phase, while the weighted three-exponential model (red solid line) was used in the isotropic phase. The three components of the decay T_{1a} (methyl, dash-dotted line), T_{1b} (methylene, dashed line), and T_{1c} (aromatic core, dotted line) are represented as well.

A more detailed overview of the relaxation mechanisms, connected to various motional processes present in the phases of the HZL 7/* sample is reported in the Supporting Information.

4. Results and Discussion

A remarkable feature found in the HZL 7/* sample is the fact that the ^1H NMR longitudinal relaxation is clearly non-monoexponential in the isotropic and N* phases, as illustrated in Figure 1a, and monoexponential in the TGB phases, as illustrated in Figure 1b. In order to analyze the behavior of the longitudinal relaxation in the isotropic and N* phases, we have introduced a three-exponential relaxation model with the assumption that these three different relaxation components, named T_{1a} , T_{1b} , and T_{1c} , are related to the methyl groups (12 protons), methylene groups (18 protons), and aromatic moiety (12 protons), respectively (see Scheme 3). Therefore, the weighting factor for each component depends on the corresponding number of protons. This assumption is supported by the fact that the spin-lattice relaxation measurements in the superconducting 100 MHz magnet showed a difference in the T_1 values of different proton groups. In addition, this assignment is consistent with results obtained by deuterium NMR studies where the R_1 values for different deuterons along the alkyl chain were first measured separately by Beckmann et al.³⁸ A similar multiexponential decay of proton magnetization was previously observed in other isotropic phases of other liquid crystals.^{39,40} As shown in Figure 1a, our three-exponential model matches the measurements quite well, while a monoexponential function does not. On the other hand (Figure 1b), a monoexponential model perfectly describes the longitudinal relaxation at lower temperatures in the TGB phases. This can be associated with the fact that spin diffusion is able to establish a single temperature over the ensemble of spins.

In Figure 2, the temperature dependencies of relaxation rates at four representative Larmor frequencies are reported. It is

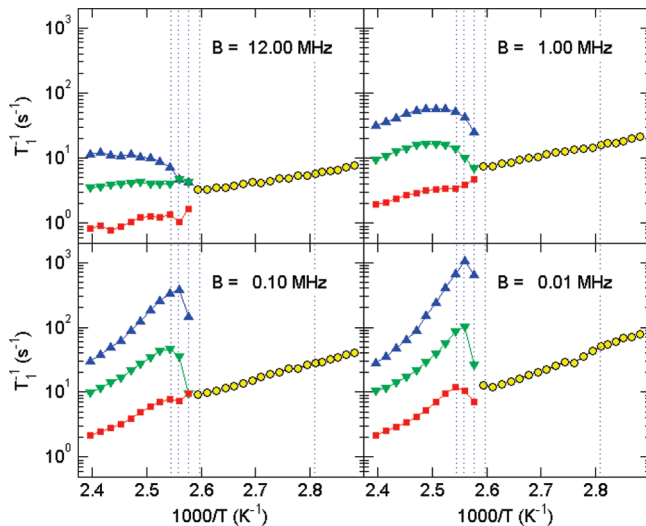


Figure 2. Temperature dependence of the proton longitudinal relaxation rates, T_1^{-1} , as a function of $1000/T$ (K^{-1}) for several frequencies: 10 kHz, 100 kHz, 1 MHz, and 12 MHz. At high temperatures (I and N^* phases), the three relaxation rate components are shown as ■ (T_{1a}^{-1}), ▼ (T_{1b}^{-1}), and ▲ (T_{1c}^{-1}). At low temperatures (TGB* phases) a single relaxation rate is reported as ○ (T_1^{-1}). The vertical dotted lines indicate the transition temperatures as given in section 2.1, biphasic regions included.

interesting to observe that in the isotropic phase the three components of the relaxation rate increase with decreasing temperature for frequencies below 1 MHz and they are approximately constant at 12 MHz. The relaxation rate in the TGB phases presents a monotonous increase by decreasing the temperature. Between the isotropic– N^* and N^* –TGBA* temperature transitions, the three components present a significantly different behavior. This coincides with the region where the two biphasic regions and the N^* phase are present. It is relevant to mention that the T_{1c} component, assigned to the molecular core, presents a more significant change in this region, in particular below 100 kHz. This may be associated with the fact that spin relaxation of the molecular core protons reflects the collective motions more prominently than the rest of the molecule, in agreement with the assignment of molecular core protons to the T_{1c} component. We should mention that in the region between the N^* phase and the TGBA* phase the distinction between mono- or three-exponential model is not as clear as in the other regions, this being compatible with the presence of the biphasic region, as also revealed by ^2H NMR measurements.^{12,13}

In the following, we present a thorough and consistent analysis of the frequency dispersions of spin–lattice relaxation, using appropriate models for each of the phases exhibited by HZL 7/*.

4.1. Isotropic Phase. The two dispersion data sets obtained in the isotropic phase at 147.8 and 123.1 °C were analyzed simultaneously using a model equation that considers the contributions of the following relaxation mechanisms: fast rotations/reorientations (Rf), translational self-diffusion (SD), molecular tumbling (slower molecular rotations/reorientations) (Rt), and order director fluctuations (ODF).

The preliminary fits of the three components made independently at each temperature revealed that the ODF contribution is negligible at 147.8 °C and should therefore be omitted from the fitting. On the contrary, at 123.1 °C, closer to the I– N^* , the formation of nematic cybotactic clusters indeed requires the inclusion of the ODF relaxation mechanism. It was also clear

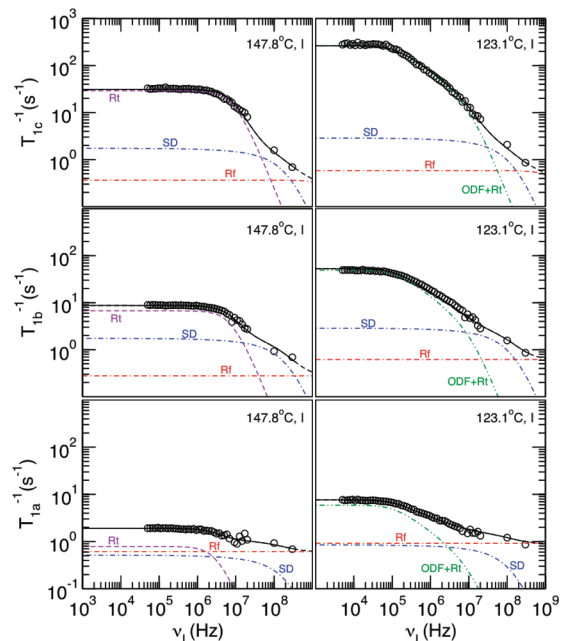


Figure 3. Frequency dependence of the proton spin–lattice relaxation rates (T_1^{-1}) for the sample HZL 7/* at 147.8 and 123.1 °C (isotropic phase). T_{1a}^{-1} , T_{1b}^{-1} , and T_{1c}^{-1} are the three relaxation rate components as described in the text. The empty circles are experimental data, and the solid black curves are the total fitting curves. Separate curves for the three main dynamic mechanisms, as presented in the text, are also displayed. The free fitting parameters are reported in Table 1.

that closer to the I– N^* phase transition the tumbling molecular motion could not be identified as an independent relaxation mechanism. As the ODF contribution also describes this type of motion when the Larmor frequency is larger than the high cutoff frequency (see the Supporting Information), the spin–lattice relaxation dispersion was interpreted in the terms of RF+SD+[ODF+Rt], with ODF+Rt considered as a single contribution. As expected, we were able to simultaneously fit all three T_1 components, belonging to the three proton groups of the HZL 7/* molecule (see Scheme 3), with the same expression, albeit with some differences in the fitting parameters. In order to reduce the number of free fitting parameters as much as possible, we made the following assumptions:

- (i) The fast rotations/reorientations process is described by a single BPP contribution with correlation times τ_{fi} and prefactors A_{fi} for the T_{1i}^{-1} components ($i = a, b, c$); the τ_{fi} are assumed to be thermally activated with activation energies E_{fi} .
- (ii) The molecular tumbling process was also described by a BPP with τ_{ti} and A_{ti} for T_{1i}^{-1} .
- (iii) The SD contribution was described by Torrey's model³³ with a common correlation time τ_d and an activation energy E_D but with different distances d_i for each component.
- (iv) The ODF+Rt contribution depends on the two cutoff frequencies $\nu_{C\min}$ and $\nu_{C\max}$ and prefactors A_{ODFi} ($i = a, b, c$), as free parameters. The best fit obtained with this model is presented in Figure 3. The fitting parameters are presented in Table 1, with activation energies of $E_{fa} = 25.8 \text{ kJ/mol}$, $E_{fb} = 44.8 \text{ kJ/mol}$, $E_{fc} = 22.69 \text{ kJ/mol}$, and $E_D = 28.2 \text{ kJ/mol}$, $n = 4.5 \times 10^{22} \text{ spins/cm}^3$, $d_a = d_b = 4 \times 10^{-10} \text{ m}$, and $d_c = 6 \times 10^{-10} \text{ m}$. The ODF contribution is only required for the analysis of the relaxation dispersion at 123.1 °C where it presents the

TABLE 1: Optimized Fitting Parameters of the ^1H NMR T_1 Sweeps Recorded in the Isotropic Phase of the HZL 7/* Sample, as Described in the Text

		147.8 °C	123.1 °C
$\tau_f (\times 10^{-11} \text{ s})$	a	2.8	4.5
	b	2.5	4.6
	c	5.6	8.3
$A_f (\times 10^9 \text{ s}^{-2})$	a	2.6	2.6
	b	2.2	2.2
	c	2.2	2.2
$\tau_t (\times 10^{-8} \text{ s})$	a	1.1	
	b	1.2	
	c	2.8	
$A_t (\times 10^8 \text{ s}^{-2})$	a	5.4	
	b	1.1	
	c	5.5	
$A_{\text{ODF}} (\times 10^4 \text{ s}^{-3/2})$	a		9.2
	b		1.7
	c		0.20
$\nu_{\text{Cmin}} (\times 10^4 \text{ Hz})$			8.8
$\nu_{\text{Cmax}} (\times 10^7 \text{ Hz})$			1.7
$\tau_D (\times 10^{-9} \text{ s})$		0.41	0.68

main relaxation mechanism in the sub-MHz frequency range for all the T_1^{-1} components, although it is clear that the T_{1c}^{-1} component (corresponding to the molecular core) is the one more sensitive to the onset of the nematic ordering. A single low cutoff frequency was used to describe the ODF behavior at low frequencies for all T_1 components.

4.2. Chiral Nematic Phase. Similar to the isotropic phase, three T_1 components of the magnetization relaxation were revealed in the N* phase. The spin–lattice relaxation rate model considers the following four contributions:

$$T_1^{-1}(\omega) = \left(\frac{1}{T_1} \right)_{\text{Rf}} + \left(\frac{1}{T_1} \right)_{\text{SD}} + \left(\frac{1}{T_1} \right)_{\text{ODF+Rt}} + \left(\frac{1}{T_1} \right)_{\text{RMTD}} \quad (3)$$

with Rf, SD, and ODF+Rt as in the case of the isotropic phase at 123.1 °C, plus the RMTD contribution associated with the rotations induced by the translational displacements along the helical axis of the N* phase (see Scheme 2). Since it is hard to establish the A_{ODF} functional dependence on temperature in the absence of independent values of the viscoelastic constants of this compound, the three $A_{\text{ODF}i}$ were considered free fitting parameters at both temperatures. The correlation times associated with the fast reorientational contribution were calculated from the values obtained in the isotropic phase taking into account the estimated activation energies (see Table 2). The A_{ti} values were also considered free parameters, as they must reflect the increased nematic order in the N* phase compared to the isotropic phase. Both cutoff frequencies in ODFs were considered free fitting parameters. In view of the specific nature of the RMTD contribution, just one correlation time τ_{RMTD} and three parameters $A_{\text{RMTD}i}$ were considered in the fitting analysis. The SD model specific for the nematic phases was included in eq 3 with τ_d as the only free parameter. The values of $d_a = 5 \times 10^{-10} \text{ m}$, $d_b = 4.5 \times 10^{-10} \text{ m}$, and $d_c = 6 \times 10^{-10} \text{ m}$ correspond to the best global fit at the single temperatures. In Figure 4, we present the best fitting curve obtained at $T = 115.6$ °C. Identically good fits were obtained at $T = 117.7$ °C. The ODF+Rt contribution is still the most important relaxation mechanism at low frequencies, especially in the case of the T_{1c}^{-1} and T_{1b}^{-1} components. The RMTD contribution is indeed neces-

TABLE 2: Optimized Fitting Parameters of the ^1H NMR T_1 Sweeps Recorded in the Cholesteric Phase of the HZL 7/* Sample, as Described in the Text

		117.7 °C	115.6 °C
$\tau_f (\times 10^{-11} \text{ s})$	a	5.0	5.2
	b	6.8	7.3
	c	9.2	9.5
$A_f (\times 10^9 \text{ s}^{-2})$	a	3.7	4.0
	b	2.7	2.6
	c	2.1	2.2
$A_{\text{ODF}} (\times 10^4 \text{ s}^{-3/2})$	a	5.4	5.2
	b	1.0	0.72
	c	0.10	0.10
$\nu_{\text{Cmin}} (\times 10^4 \text{ Hz})$		~0.01	~0.01
$\nu_{\text{Cmax}} (\times 10^7 \text{ Hz})$		1.6	0.78
$\tau_{\text{RMTD}} (\times 10^{-6} \text{ s})$		1.3	1.8
$A_{\text{RMTD}i} (\times 10^6 \text{ s}^{-2})$	a	190	150
	b	15	8.1
	c	1.5	0.01
$\tau_D (\times 10^{-9} \text{ s})$		2.5	2.8

sary in the low frequency range and can be clearly detected in the T_{1c}^{-1} and T_{1b}^{-1} components. T_{1a}^{-1} is less sensitive to this type of motion, as expected for the methyl groups. On the other hand, the assumption that T_{1c}^{-1} is associated with the molecular core is consistent with the fact that the dispersion of this component is clearly more affected by both ODF and RMTD relaxation contributions (see Table 2). It is interesting to observe that the high cutoff frequency of the ODF+Rt decreases with decreasing temperature. As suggested above, this cutoff frequency reflects not only the short wavelength cutoff in the ODF modes but also the fact that the correlation time for the molecular tumbling increases with decreasing temperature. The correlation time associated with the RMTD mechanism in the chiral nematic phase presents a slight increase consistent with slowing down of this motion when the temperature decreases.

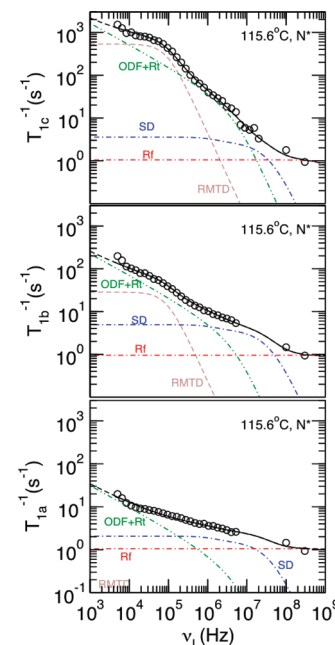


Figure 4. Frequency dependence of the proton spin–lattice relaxation rates (T_1^{-1}) for the sample HZL 7/* at 115.6 °C (N* phase). T_{1a}^{-1} , T_{1b}^{-1} , and T_{1c}^{-1} are the three relaxation rate components as described in the text. The empty circles are experimental data, and the solid black curves are the total fitting curves. Separate curves for the three main dynamic mechanisms, as presented in the text, are also displayed. The free fitting parameters are reported in Table 2.

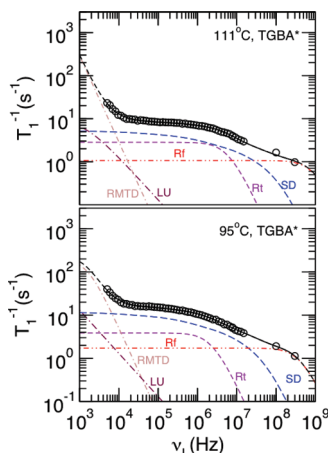


Figure 5. Frequency dependence of the proton spin–lattice relaxation rates (T_1^{-1}) for the sample HZL 7/* at 95 and 111 °C (TGBA* phase). The empty circles are experimental data, and the solid black curves are the total fitting curves. Separate curves for the three main dynamic mechanisms, as presented in the text, are also displayed. The free fitting parameters are reported in Table 3.

4.3. TGBA* Phase. As discussed above, the magnetization decay in the TGB* phases is monoexponential. The analysis of the relaxation dispersion curves reflects the specific structure of this phase: since the structure within the TGBA* blocks (see Scheme 1) is similar to that of a SmA phase, it is reasonable to expect the collective motions as layer undulations.²³ In the asymptotic limit at high frequencies, the LUs can no longer be interpreted as the local molecular tumbling, as in the case of ODFs. Therefore, the molecular tumbling must be considered as an independent relaxation mechanism. The total relaxation rate model in a first approximation is

$$T_1^{-1}(\omega) = \left(\frac{1}{T_1}_{\text{Rf}} \right) + \left(\frac{1}{T_1} \right)_{\text{SD}} + \left(\frac{1}{T_1} \right)_{\text{Rt}} + \left(\frac{1}{T_1} \right)_{\text{LU}} + \left(\frac{1}{T_1} \right)_{\text{RMTD}} \quad (4)$$

As the magnetization in the TGB phases decays monoexponentially, the number of free fitting parameters in eq 4 is reduced to a single relaxation rate T_1^{-1} . The match between the fitting parameters in the TGB phases and those obtained in the isotropic and cholesteric phases is not expected because T_1^{-1} now reflects the dynamics of all protons in the molecule, while the T_{1a}^{-1} , T_{1b}^{-1} , and T_{1c}^{-1} components are connected to the separate proton groups. In the model expressed by eq 4, τ_d , τ_f , τ_t , τ_{RMTD} , A_t , A_f , A_{LU} , and A_{RMTD} were considered free fitting parameters, while a fixed value of $d = 4.5 \times 10^{-10}$ m was used, compatible with the values d_a , d_b , and d_c , obtained in the I and N* phase fits. In Figure 5, the best fit obtained in the TGBA* phase at 95 and 111 °C is shown. The free fitting parameters are presented in Table 3. It is worth noticing that the values of the fitting parameters are very similar to those referred to in the literature for the SmA phase, except that in the low frequency regime the T_1^{-1} trend is better explained by a stronger contribution of RMTD relaxation mechanism. This result can be considered very significant, since the large temperature range of stability of the TGBA* phase of the HZL 7/*, rare in other TGB systems investigated so far, makes the present analysis much stronger than previous studies.^{11,24} In our model, LUs are included as a minor contribution in the low frequency range. Translational self-diffusion dominates the relaxation dispersion in the inter-

TABLE 3: Optimized Fitting Parameters of the ^1H NMR T Sweeps Recorded in the TGBA* Phase of the HZL 7/* Sample, as Described in the Text

	111 °C	95 °C
$\tau_f (\times 10^{-11} \text{ s})$	10	23
$A_f (\times 10^9 \text{ s}^{-2})$	2.1	1.5
$\tau_t (\times 10^{-8} \text{ s})$	1.6	4.0
$A_t (\times 10^8 \text{ s}^{-2})$	0.36	0.19
$A_{\text{LU}} (\times 10^4 \text{ s}^{-2})$	1.3	1.3
$\tau_{\text{RMTD}} (\times 10^{-6} \text{ s})$	100	100
$A_{\text{RMTDc}} (\times 10^6 \text{ s}^{-2})$	0.59	1
$\tau_D (\times 10^{-9} \text{ s})$	1.1	2.4

mediate frequency regime, as observed in many other SmA phases,²³ while fast overall rotations and internal reorientation motions are relevant only in the high frequency range. In this phase, the molecular tumbling relaxation process appears as a minor contribution in the intermediate frequency range and it is more important at 111 °C than at 95 °C due to the vicinity of the N*–TGBA* transition. Dielectric measurements on the HZL 7/* compound revealed that typical soft modes¹² are present within the TGBA* blocks, similarly to what was observed in the SmA phases. However, dielectric results reflect the strong influence of the external electrical field on the TGBA* phase structure: a reversible TGBA*–SmA phase transition can be indeed induced by applying/removing the voltage.¹² This phenomenon is not present in our study, since the TGBA* structure cannot be unwound by magnetic fields lower than 4.2 T, as clearly shown by previous ^2H NMR studies.¹³ For this reason, a direct comparison between ^1H NMR relaxometry and dielectric¹² results could be misleading. In our previous investigation on the HZL 7/* sample by means of ^2H and ^{13}C NMR spectroscopy,¹³ we could get information about the phase structure and local orientational order S within the TGBA* blocks which was found to be typical of TGBA* phases. Moreover, the ^2H NMR spectral line shape¹⁵ at magnetic fields lower than 4.2 T revealed that the jump diffusion of molecules along the TGB pitch (namely, from one TGBA* block to the next one) is in the intermediate–slow regime, thus confirming the results obtained in the present ^1H NMR relaxation analysis.

4.4. TGBC* Phases. As mentioned in section 1, HZL 7/* has two TGBC* phases, denoted as TGBC₁* and TGBC₂*, characterized by in-blocks SmC* phase structure (see Scheme 1). As observed by previous investigation,¹³ the two TGBC* phases are very sensitive to applied magnetic and electric fields, leading to unwinding of the SmC* phase structure within the TGBC* blocks whenever a critical field is exceeded. However, as suggested by previous ^2H NMR studies,¹³ the TGBC* superstructure is not unwound by magnetic fields below 4.2 T but only partially distorted. The differences between the two TGBC* phases detected by optical texture analysis, dielectric spectroscopy,¹² or ^2H NMR line-shape analysis are rather tiny.¹⁵ In fact, they can be considered as two different variants of the TGBC* structure reported in Scheme 1. The basic features of these two phases can be summarized here:

- (i) the presence of the helical SmC*-phase structure (and molecular tilt) within each TGBC* block,
- (ii) a rather short TGB pitch ($\sim 1 \mu\text{m}$) for the TGBC₁* and much longer for the TGBC₂*,
- (iii) a rather distorted distribution of orientations in the case of TGBC₁* (probably due to frustration of the phase in the presence of magnetic fields $B \geq 4$ T) and a substantial undistorted structure in the case of the TGBC₂*, at magnetic fields of ~ 4 T.

TABLE 4: Optimized Fitting Parameters of the ^1H NMR T_1 Sweeps Recorded in the TGBC* Phases of the HZL 7/* Sample, as Described in the Text

	TGBC ₁ *	TGBC ₂ *
	60 °C	40 °C
$\tau_f (\times 10^{-11} \text{ s})$		
$A_f (\times 10^9 \text{ s}^{-2})$		
$\tau_t (\times 10^{-8} \text{ s})$	0.15	
$A_t (\times 10^8 \text{ s}^{-2})$	3.3	
$A_{\text{cDF}} (\times 10^4 \text{ s}^{-3/2})$	1.3	
$A_{\text{LU}} (\times 10^4 \text{ s}^{-2})$		3980
$\nu_{\text{Cmin}} (\times 10^4 \text{ Hz})$	8.6	4.0
$\nu_{\text{Cmax}} (\times 10^7 \text{ Hz})$		1.9
$\tau_{\text{RMTD}} (\times 10^{-6} \text{ s})$	0.49	19
$A_{\text{RMTDc}} (\times 10^6 \text{ s}^{-2})$	0.55	55
$\tau_D (\times 10^{-9} \text{ s})$	4.9	0.28

- (iv) in both TGBC* phases, the dielectric relaxation is dominated by the Goldstone modes similarly to SmC* phases, but the TGBC* phases are easily converted to a SmC* phase by applying electric fields at low voltage.

In the analysis of the ^1H NMR relaxation rates in the TGBC₁* phase (at $T = 60^\circ\text{C}$), we first considered the model identical to the one used for the TGBA* phase (see eq 4). However, the parameters obtained by this procedure were not compatible with those obtained for the other phases, e.g., the LU mechanism required a rather unrealistically low value for the high cutoff frequency. Since it is possible to observe in-layer fluctuations of the tilting direction in the SmC* phase (cDF), a modified model was considered for the analysis of the TGBC* phases.³⁵

$$T_1^{-1}(\omega) = \left(\frac{1}{T_1}\right)_{\text{SD}} + \left(\frac{1}{T_1}\right)_{\text{Rf}} + \left(\frac{1}{T_1}\right)_{\text{cDF+Rf}} + \left(\frac{1}{T_1}\right)_{\text{RMTD}} \quad (5)$$

As in the case of the nematic order director fluctuations, the range of in-layer c -director fluctuation (cDF) modes is limited and, as a consequence, the high cutoff frequency is related to the fluctuation mode with a wave vector corresponding to the molecular dimensions. This type of fluctuations is related to the molecular fast reorientations around the normal to the layers. This superposition of contributions in the high frequency part of the spin–lattice relaxation dispersion makes it difficult to separately determine the values of the correlation time for the fast reorientational (Rf) contribution and the value of the high cutoff frequency of the cDF relaxation mechanism. Therefore, the final model (see eq 5) considers the sum cDF+Rf as a single motional contribution.

The fitting parameters match those of the TGBA* phase except for τ_f and A_f and those associated to the LUs were replaced by those associated with the cDFs, namely, A_{cDF} , ν_{Cmin} , and ν_{Cmax} . The best fit with the parameters displayed in Table 4 is presented in Figure 6. The cDF and SD relaxation mechanisms give more important contributions at intermediate frequencies, whereas the RMTD seems to be the most important relaxation contribution in the low frequency range. The layer undulations do not significantly contribute to the total relaxation, so they can be neglected.

The ^1H NMR relaxation dispersions of HZL 7/* in the TGBC₂* phase recorded at 40 °C are reported in Figure 7. As it can be noticed, the T_1 trend observed at 40 °C is clearly different from the one observed at 60 °C, as the slope at intermediate frequencies demonstrates a $T_1^{-1} \sim \omega^{-1}$ dependence. A tentative model includes a contribution from fast rotations/

reorientations plus translational self-diffusion, a contribution from layer undulations, and a contribution from RMTD:

$$T_1^{-1}(\omega) = \left(\frac{1}{T_1}\right)_{\text{SD+Rf}} + \left(\frac{1}{T_1}\right)_{\text{LU}} + \left(\frac{1}{T_1}\right)_{\text{RMTD}} \quad (6)$$

This model explains the main dispersion features quite well, although the quality of the fit is not perfect at high frequencies. The contribution of molecular tumbling could not be estimated, as it is hidden by the dominating LU relaxation dispersion. On the other hand, the inclusion of another relaxation mechanism in the fit would not improve the fit's quality significantly. The best fitting parameters are presented in Table 4; a fixed value $d = 4.5 \times 10^{-10} \text{ m}$ was also considered. Additional experimental points above 20 MHz could help to clarify the relaxation mechanisms. However, as observed from ^2H NMR studies,¹³ at high fields, the TGBC* structures are highly distorted,¹⁵ thus limiting the possibility to investigate the undistorted TGBC* phase structures in the high frequency regime. At this stage, however, some conclusions can be drawn. In fact, the differences observed between the spin–lattice relaxation dispersion in the two TGBC* phases, in particular in the intermediate and low frequency regimes, are consistent with the dielectric spectroscopy results, where an anomaly in the $\Delta\epsilon(T)$ and $f_i(T)$ was observed at the TGBC₁*–TGBC₂* phase transition.¹² In addition to the previous dielectric study, the analysis of ^1H NMR

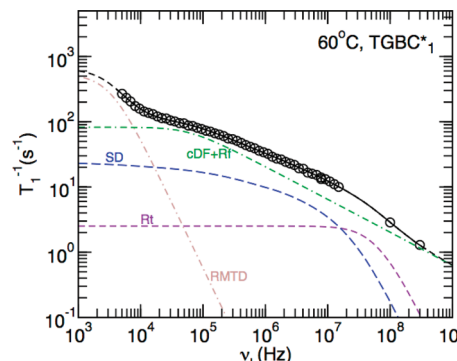


Figure 6. Frequency dependence of the proton spin–lattice relaxation rates (T_1^{-1}) for the sample HZL 7/* at 60 °C (TGBC₁* phase). The empty circles are experimental data, and the solid black curves are the total fitting curves. Separate curves for the three main dynamic mechanisms, as presented in the text, are also displayed. The free fitting parameters are reported in Table 4.

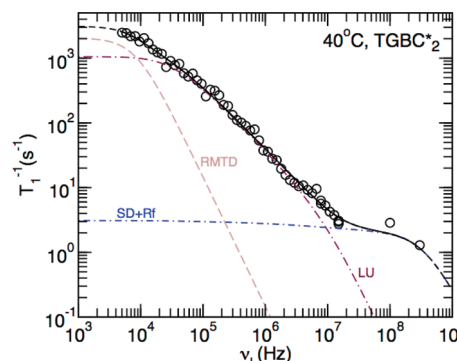


Figure 7. Frequency dependence of the proton spin–lattice relaxation rates (T_1^{-1}) for the sample HZL 7/* at 40 °C (TGBC₂* phase). The empty circles are experimental data, and the solid black curves are the total fitting curves. Separate curves for the three main dynamic mechanisms, as presented in the text, are also displayed. The free fitting parameters are reported in Table 4.

dispersion curves allowed us to identify the motional contributions active in the two phases and the differences in the characteristic parameters, as clearly reported in Table 4.

5. Conclusions

In this work, we present and discuss a detailed ^1H NMR relaxation study on the HZL 7/* liquid crystal exhibiting the chiral nematic and several TGB phases. In the isotropic and N^* phases, a three-exponential magnetization decay was observed and it was explained by consistently assigning three experimental relaxation rates to specific molecular groups, namely, molecular core, methyl, and methylene groups. The simultaneous fit of all relaxation rate dispersions in the isotropic phase was performed taking into account the pretransitional effect interpreted in terms of the nematic order and the formation of cybotactic nematic clusters close to the isotropic–nematic phase transition. The simultaneous analysis of the three T_1 components in the N^* phase shows that the molecular reorientations induced by the molecular translational self-diffusion along the helical axis are more relevant for the relaxation associated with the molecular core proton spin subsystem and almost irrelevant for the other two T_1 components assigned to the molecular methyl groups. In all the TGB phases, a monoexponential magnetization decay was observed. The ^1H spin–lattice dispersion in the TGBA* phase is strongly dominated by the translational self-diffusion relaxation mechanism over a broad frequency range, as observed for many smectic A phases,²³ except that layer undulations are less relevant for the relaxation than the RMTD contribution associated with the diffusion process across the twist grain boundaries, which may be identified as a distinctive relaxation process in the TGBA*. In the TGBC₁* phase, the T_1 dispersion presents a strong contribution of a relaxation mechanism with a $T_1^{-1} \sim \omega^{-1/2}$ law that can be associated with the in-layer tilt direction fluctuations. In the TGBC₂* phase, the T_1 dispersion is clearly different from the one observed for the TGBC₁* phase. In fact, the T_1 profile has a linear frequency dependence over a large frequency range. This was associated with a much stronger contribution of layer undulations than for the other TGBC₁* and TGBC₂* phases. Further experimental work is needed in order to clarify the small differences between TGBC₁* and TGBC₂* phases and to shed more light on the interesting molecular dynamics of these challenging mesophases.

Acknowledgment. This work was partly supported by the Italian MIUR, project PRIN 2005, and by the ESF-COST Action D35 WG0013/05. Author V.D. is grateful to the COST for Grant No. COST-STSM-D35-02629. P.J.S. wishes to thank Fabian Vaca Chaves for his assistance on the 300 MHz measurements.

Supporting Information Available: A complete section about the theory of ^1H NMR relaxation (S1) and a full table with the best fitting parameters obtained from the fitting of ^1H NMR relaxation of HZL 7/* in its mesophases (S2). This material is available free of charge via the Internet at <http://pubs.acs.org>.

References and Notes

- (1) Kamien, R. D.; Selinger, J. V. *J. Phys: Condens. Matter* **2001**, *13*, R1.
- (2) Goodby, J. W. *Curr. Opin. Colloid Interface Sci.* **2002**, *7*, 326.
- (3) Crooker, P. P. *Liq. Cryst.* **1989**, *5*, 751. Kitzerow, H. S. *ChemPhysChem* **2006**, *7*, 63.
- (4) Renn, S. R.; Lubensky, T. C. *Phys. Rev. A* **1988**, *38*, 2132.
- (5) Goodby, J. W.; Waugh, M. A.; Stein, S. M.; Chin, E.; Pindak, R.; Patel, J. S. *Nature* **1989**, *337*, 449.
- (6) (a) Galerne, Y. *Eur. Phys. J. E* **2000**, *3*, 355. (b) Brunet, M.; Naivailles, L.; Clark, N. A. *Eur. Phys. J. E* **2002**, *7*, 5. (c) Naivailles, L.; Garland, C. W.; Nguyen, H. T. *J. Phys. II* **1996**, *6*, 1243. (d) Kundagrami, A.; Lubensky, T. C. *Phys. Rev. E* **2003**, *68*, 060703 (R). (e) Ismaili, M.; Bougrioua, F.; Isaert, N.; Legrend, C.; Nguyen, H. T. *Phys. Rev. E* **2001**, *65*, 011701.
- (7) Ribeiro, A. C.; Oswald, L.; Nicoud, J. F.; Guillon, D.; Galerne, Y. *Eur. Phys. J. B* **1998**, *1*, 503.
- (8) Barois, P.; Heidelbach, F.; Naivailles, L.; Nguyen, H. T.; Nobili, M.; Petit, M.; Pindak, R.; Riekel, C. *Eur. Phys. J. B* **1999**, *11*, 455.
- (9) Ybert, C.; Naivailles, L.; Pansu, B.; Rieutord, F.; Nguyen, H. T.; Barois, P. *Europhys. Lett.* **2003**, *63*, 840.
- (10) Catalano, D.; Chiezza, L.; Domenici, V.; Geppi, M.; Veracini, C. A. *J. Phys. Chem. B* **2003**, *107*, 10104.
- (11) Zhang, J.; Domenici, V.; Veracini, C. A.; Dong, R. Y. *J. Phys. Chem. B* **2006**, *110*, 15193.
- (12) Novotna, V.; Kaspar, M.; Domenici, V.; Hamplova, V.; Glogarova, M.; Bilkova, P.; Pocieca, D. *Liq. Cryst.* **2008**, *35*, 287.
- (13) Domenici, V.; Veracini, C. A.; Novotna, V.; Dong, R. Y. *ChemPhysChem* **2008**, *9*, 556.
- (14) (a) Nair, G. G.; Prasad, S. K.; Yelamaggad, C. V. *Ferroelectrics* **2002**, *277*, 431. (b) Petit, M.; Nobili, M.; Barois, P. *Eur. Phys. J. B* **1998**, *6*, 341.
- (15) Domenici, V.; Veracini, C. A.; Hamplova, V.; Kaspar, M. *Mol. Cryst. Liq. Cryst.* **2008**, *495*, 133.
- (16) Dodge, M. R.; Vij, J. K.; Cowling, S. J.; Hall, A. W.; Goodby, J. W. *Liq. Cryst.* **2005**, *32*, 1045.
- (17) Adorjan, A.; Stojadinovic, S.; Sukhomlinova, L.; Twieg, R.; Sprunt, S. *Phys. Rev. Lett.* **2003**, *90*, 035503.
- (18) Luckhurst, G. R.; Veracini, C. A., Eds. *The Molecular Dynamics of Liquid Crystals*; NATO ASI Series; Kluwer Academic: Dordrecht, 1989; Vol. 431, Chapter 7.
- (19) Domenici, V.; Veracini, C. A. Dynamics of Liquid Crystals by means of Deuterium NMR relaxation. In *Nuclear Magnetic Resonance of Liquid Crystals*; Dong, R. Y., Ed.; Publisher World Scientific Publishing Co.: Singapore, 2009; Chapter 8.
- (20) Schmid-Rohr, K.; Spiess, H. W. *Multidimensional Solid-state NMR and Polymers*; Academic Press: London, 1994.
- (21) Dong, R. Y. *Thin Solid Films* **2008**, *517*, 1367.
- (22) Noack, F. *Prog. Nucl. Magn. Reson. Spectrosc.* **1986**, *18*, 171.
- (23) Sebastião, P. J.; Cruz, C.; Ribeiro, A. C. Advances in Proton NMR Relaxometry in Thermotropic Liquid Crystals. In *Nuclear Magnetic Resonance of Liquid Crystals*; Dong, R. Y., Ed.; Publisher World Scientific Publishing Co.: Singapore, 2009; Chapter 6.
- (24) Figueirinhas, J. L.; Ferraz, A.; Ribeiro, A. C.; Noack, F.; Nguyen, H. T. *J. Phys. II* **1997**, *7*, 79.
- (25) Dong, R. Y. *Annu. Rep. NMR Spectrosc.* **2004**, *53*, 67.
- (26) Kimmich, R.; Anoardo, E. *Prog. Nucl. Magn. Reson. Spectrosc.* **2004**, *44*, 257.
- (27) <http://fitter.ist.utl.pt>.
- (28) Abragam, A. *The Principles of Nuclear Magnetism*; Clarendon Press: Oxford, U.K., 1961.
- (29) Dong, R. Y. *Nuclear Magnetic Resonance of Liquid Crystals*; Springer-Verlag: New York, 1997.
- (30) Vilfan, M.; Apih, T.; Sebastiao, P. J.; Lahajnar, G.; Zumer, S. *Phys. Rev. E* **2007**, *76*, 051708.
- (31) Kimmich, R.; Weber, H. W. *Phys. Rev. B* **1993**, *47*, 11788.
- (32) Bloembergen, N.; Purcell, E. M.; Pound, R. V. *Phys. Rev.* **1948**, *73*, 679.
- (33) Torrey, H. C. *Phys. Rev.* **1953**, *92*, 962.
- (34) Zumer, S.; Vilfan, M. *Phys. Rev. A* **1978**, *17*, 424. Vilfan, M.; Zumer, S. *Phys. Rev. A* **1980**, *21*, 672.
- (35) Carvalho, A.; Sebastião, P. J.; Ribeiro, A. C.; Nguyen, H. T.; Vilfan, M. *J. Chem. Phys.* **2001**, *115*, 10484.
- (36) Vilfan, M.; Blinc, R.; Dolinska, J.; Ipavec, M.; Lahajnar, G.; Zumer, S. *J. Phys. (Paris)* **1983**, *44*, 1179.
- (37) Sebastião, P. J.; Sousa, D.; Ribeiro, A. C.; Vilfan, M.; Lahajnar, G.; Seliger, J.; Zumer, S. *Phys. Rev. E* **2005**, *72*, 61702.
- (38) Beckmann, P. A.; Emsley, J. W.; Luckhurst, G. R.; Turner, D. L. *Mol. Phys.* **1986**, *59*, 97.
- (39) Hayward, R. J.; Packer, K. J. *Mol. Phys.* **1973**, *26*, 1533.
- (40) Grande, S.; Heinze, E.; Losche, A. *Phys. Lett.* **1976**, *58A*, 2.